

# Next-Generation Teleophthalmology: AI-enabled Quality Assessment Aiding Remote Smartphone-based Consultation

Dhruv Srikanth<sup>1</sup>, Jayang Gurung<sup>2</sup>, N Satya Deepika<sup>1</sup>, Vineet Joshi<sup>2</sup>, Pravin Vaddavalli<sup>2</sup>, Soumya Jana<sup>1</sup>

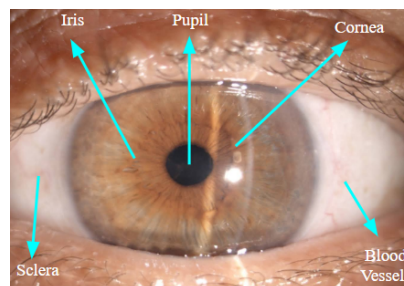
**Abstract**—Blindness and other eye diseases are a global health concern, particularly in low- and middle-income countries like India. In this regard, during the COVID-19 pandemic, teleophthalmology became a lifeline, and the Grabi attachment for smartphone-based eye imaging gained in use. However, quality of user-captured image often remained inadequate, requiring clinician vetting and delays. In this backdrop, we propose an AI-based quality assessment system with instant feedback mimicking clinicians’ judgments and tested on patient-captured images. Dividing the complex problem hierarchically, here we tackle a nontrivial part, and demonstrate a proof of the concept.

**Keywords:** Teleophthalmology, Automated image quality assessment, Smartphone-based teleconsultation.

## I. INTRODUCTION

Early detection of sight-threatening disorders and prompt treatment help preserve visual function and potentially prevent blindness [1]. Unfortunately, remote rural areas are often more severely affected. In overcoming access barriers and preventing delays (especially during the COVID-19 pandemic), smartphone-based teleconsultation has proven effective. In general, teleophthalmology not only increases the reach but also reduces treatment/other costs, conserves hospital resources and helps reduce the carbon footprint [2]. Now, can teleophthalmology provide outcomes similar to those traditionally obtained in hospitals?

During a patient’s physical visits, an ophthalmologist usually requires high-quality slitlamp images of the eye captured by trained operators, such as Fig. 1(a), for diagnosis and treatment response monitoring. Thus, assuming an in-person prior visit and availability of reference slitlamp images, teleophthalmology requires mechanisms to ensure sufficient quality in smartphone-based self-captured eye images so that treatment response can reliably be monitored. As an aid, a custom-made app-based universal smartphone adapter, Grabi™, has recently been reported [3]. As shown in Figs. 1(b) and 1(c), it facilitates capture of suitably magnified well-illuminated images of the anterior segment of the eye by maintaining appropriate direction and distance. As seen in Figs. 1(d) and 1(e), a Grabi image can be almost as informative as a slitlamp image. While patients were trained during hospital visits and found to gradually improve at image capturing, not all Grabi images turned out to be of satisfactory quality. Clinicians needed to vet those images and sometimes request re-capture, wasting time and effort. As a potential remedy, we propose to automate the process by assessing the quality of Grabi eye images using artificial



(a)



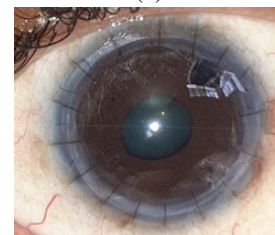
(b)



(c)



(d)



(e)

Fig. 1: (a) Labelled slitlamp image of anterior segment of human eye, (b) Grabi universal attachment fixed on dummy smartphone, (c) Grabi assisted eye image capture, (d) and (e) Slitlamp and Grabi images, respectively, of the same eye.

intelligence (AI) algorithms so that the patient obtains an immediate feedback on the need to re-capture.

## II. MATERIALS AND METHODS

### A. Problem Statement and Approach

Clinicians assess quality of an anterior segment image of the eye based on various considerations. (1) Presence of eye: A satisfactory image must include an open eye. (2) Lighting: A satisfactory image must be adequately lit, and should not suffer from large variations in pixel intensity, low average

<sup>1</sup>Indian Institute of Technology Hyderabad, Telangana, India.

<sup>2</sup>L V Prasad Eye Institute, Hyderabad, Telangana, India.

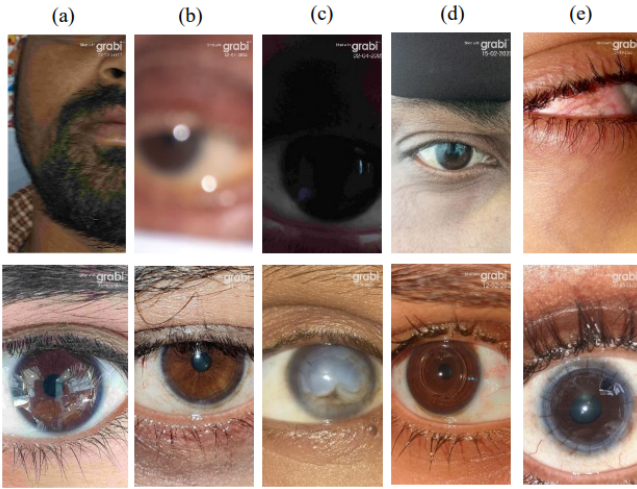


Fig. 2: Ten representative Grabi images of the anterior segment with effect of specific factors illustrated columnwise: (a) presence of eye, (b) focus, (c) illumination, (d) magnification, (e) completeness of cornea; top panel – unsatisfactory images, bottom panel – satisfactory images.

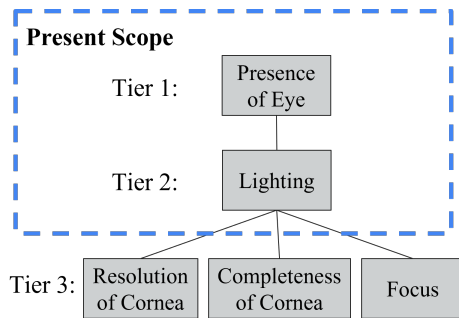


Fig. 3: Quality assessment of self-captured Grabi images: Hierarchical solution approach.

pixel intensity, and visible reflections of the surrounding environment (possibly due to improper camera flash). (3) Resolution of cornea: The distance between the smartphone and the eye should be such that the eye in the image appears in sufficient size. (4) Completeness of cornea: The Cornea, the region of maximum clinical importance, should be fully represented in the captured image. (5) Focus: Key regions such as pupil periphery, iris periphery, iris striations, conjunctival blood vessels, and artificial structures such as sutures and grafts should appear distinct and sharp, even when certain eye details may be (inherently) blurry.

At this point, refer to Fig. 2 for representative unsatisfactory (top row) and satisfactory (bottom row) images captured by Grabi-assisted smartphone camera corresponding to each of the above considerations (columnwise). However, clinicians place certain priorities on those considerations, and do not treat those as equally important. Presence of an eye is the most important consideration in the sense that an image is unsatisfactory without it. If the eye is present, lighting takes the next priority so that an inadequately illuminated image

is deemed unsatisfactory. Finally, an image with a well-lit eye present is considered usable if at least two out of the remaining three considerations are fully met, while the third consideration is met only per a relaxed standard.

Now, our task boils down to mimicking clinicians’ assessment of image quality using AI algorithms. To this end, we replicate the aforesaid hierarchy in clinical logic, and propose to verify presence of an eye in Tier 1, adequate illumination in Tier 2, and adequate resolution, completeness of cornea and satisfactory focus in parallel in Tier 3, as depicted in Fig. 3. Presently, we take up Tiers 1 and 2 only, deferring Tier 3 as future work. A detailed flowchart is presented in Fig. 4, where the parts corresponding to the future Tier 3 have been dimmed.

### B. Data Collection and Data Preparation

Either the patient or an associate captures an image of the desired eye at home using the Grabi attachment and the Grabi app on a smartphone, and uploads it to the Grabi cloud. From there, we randomly picked images of varying quality to populate a dataset to be used in present experimentation. Here, we ignored metadata such as camera parameters/specifications, image resolution, aspect ratio, flash usage, and imaging environment. Each constituent image was labelled either satisfactory (positive) or unsatisfactory (negative) in relation to presence of eye, as well as separately to suitable lighting. The presence-of-eye (Tier 1) and suitable-lighting (Tier 2) detectors were developed separately, using 5200 (with 3700 with the label eye present) and 4100 (with 3000 labeled suitably illuminated) images, respectively. Each image was resized to  $224 \times 224$  (zero padded when necessary), mean subtracted and normalized as depicted in Fig. 4.

The aforementioned detectors were tested in a hierarchical configuration, with the Tier 2 detector operating only on images classified as positive (eye present) by the Tier 1 detector. Analogously, a separate test set of 300 images was also labeled hierarchically: 100 without eye present, and of the 200 with the eye present, 100 each had suitable and unsuitable illumination.

### C. Proposed AI-based Tools and Solutions

1) *General engineering principle:* Both the presence-of-eye and the suitable-lighting detectors were realized using a particular residual CNN (convolutional neural network) architecture with 2 output nodes in each case [4], in view of its reported efficacy in classification tasks and relatively light weight. Specifically, as our base model of either detector, we used a ResNet-18 model pretrained on ImageNet benchmark object detection dataset, because of the representation of the home environment at which present eye images are expected to be captured. For each detector, suitable layers of the base model were trained using respective training data. More generally, each detector was individually developed and tested using the corresponding dataset, via the sequential process of training, validation and testing. Finally, those detectors were tested in the intended hierarchical configuration on another test set specially constructed for this purpose.

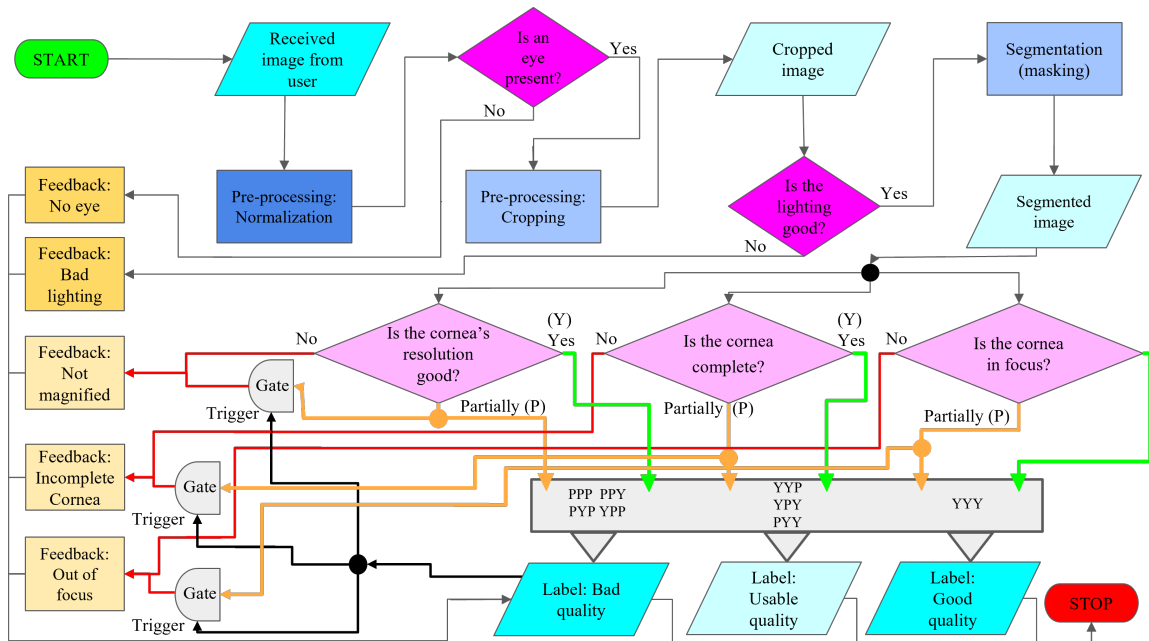


Fig. 4: Flowchart of the envisaged solution for end-to-end image quality assessment.

2) *Specific considerations and variants*: We considered two variants of the presence-of-eye detector: Pertaining to the base ResNet-18 model, (i) only weights at the final layer are learnt keeping other weights at their pretrained values, and (ii) all weights/parameters are learnt. Two variants of the suitable-lighting detectors too were considered: Input data underwent (i) no transformation, and (ii) 2-level Haar wavelet transform [5]. In either variant, all weights of the base ResNet-18 model were learnt afresh.

3) *Performance Metrics*: Further, while we make use of  $Accuracy = (TP + TN) / (TP + TN + FP + FN)$  as a performance metric ( $TP$ ,  $TN$ ,  $FP$  and  $FN$ , respectively, being the counts of true positive, true negative, false positive and false negative cases), it presently conveys limited meaning due to (i) possible class imbalance and (ii) the fact that a positive case being misclassified as a negative one (prompting unnecessary image retake by user) is less costly than the other way round (prompting significant wastage of clinician's as well as patient's time). In contrast, the  $P4$  metric [6], defined by

$$\frac{4}{P4} = \frac{1}{Precision} + \frac{1}{Recall} + \frac{1}{Specificity} + \frac{1}{NPV},$$

i.e., the harmonic mean of  $Precision = TP / (TP + FP)$ ,  $Recall = TP / (TP + FN)$ ,  $Specificity = TN / (TN + FP)$  and negative predictive value  $NPV = TN / (TN + FN)$ , is insensitive to data imbalance and relative weightage of positive and negative classes. However, in order to cater specifically to issue (ii), in addition to (i), we coined a custom metric defined by the harmonic mean of  $Precision$  and  $Specificity$

$$\frac{2}{Custom} = \frac{1}{Precision} + \frac{1}{Specificity},$$

which de-emphasizes  $FN$  (that simply allows image retake).

4) *Training, validation and testing*: Each of the aforementioned detectors were trained, validated and tested on the corresponding dataset. The respective dataset was split in the ratio 8:1:1 into training, validation and test subsets. The above was performed 5 times randomly. Each time, model parameters/weights were learned based on the training subset by minimizing cross-entropy loss using stochastic gradient descent. Further, after each epoch, training and validation losses were recorded with the aim of picking the parameters learnt at the epoch with the minimum validation loss.

For the parameters so chosen, we considered the detector validation performance in terms of the Custom Score, defined earlier. Further, for each model, we considered two hyperparameters, namely, learning rate ( $LR$ ) and momentum ( $M$ ). Further, viewing optimally learnt network weights, and hence the Custom (validation) Score, as functionals of the chosen hyperparameter pair, We chose the pair that maximized the said score. Test performance was reported in terms of the mean and the standard deviation (over the test subset across the 5 random iterations) of the corresponding classification scores measured by the chosen performance metrics.

The presence-of-eye and suitable-lighting detectors were finally arranged in the hierarchical configuration shown in Fig. 3 and 4, tested on the hierarchically labelled dataset at hand (described in Sec. II-B), and the performance was reported in terms of the confusion matrix and aforementioned related indices for end-to-end outcome (i.e., good versus poor quality). For any image deemed to be of poor quality, we generated the potential feedback on the underlying quality issue (see Fig. 4).

### III. EXPERIMENTAL RESULTS & DISCUSSION

For the presence-of-eye detector, the test performance was superior when all layers were trained (compared to

TABLE I: Independent testing results for 'presence of eye' and 'lighting' features

Dataset	Parameters Trained	Transforms	Accuracy (Mean $\pm$ StdDev)	P4 Score (Mean $\pm$ StdDev)	Custom Score (Mean $\pm$ StdDev)	Learning Rate	Momentum
Eye Present	Last FC Layer	None	96.532% $\pm$ 0.6332%	0.957 $\pm$ 0.0082	0.951 $\pm$ 0.0144	0.0002	0.95
	All Layers	None	<b>96.840% <math>\pm</math> 0.4656%</b>	<b>0.961 <math>\pm</math> 0.0061</b>	<b>0.957 <math>\pm</math> 0.0071</b>	0.0001	0.99
Lighting	All Layers	None	<b>88.193% <math>\pm</math> 1.2096%</b>	<b>0.849 <math>\pm</math> 0.0180</b>	<b>0.862 <math>\pm</math> 0.0391</b>	0.0002	0.99
	All Layers	Wavelet	88.145% $\pm$ 1.0492%	0.841 $\pm$ 0.0185	0.814 $\pm$ 0.0385	0.0002	0.99

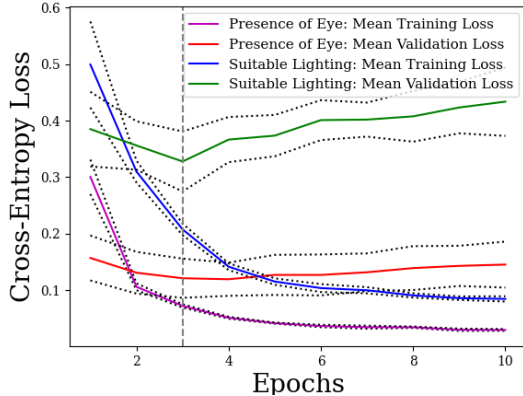


Fig. 5: Cross-validation loss plot for ResNet-18 (all layers trained without transform): (a) Presence-of-eye detector; (b) Suitable lighting detector. Dotted black lines bounding each loss curve denote  $mean \pm standard\ deviation$  for the respective curve.

when only last FC layer was trained, see Table I). For the suitable-lighting detector, the test performance of the variant where no transform was applied turned out to be superior in comparison to the one with Wavelet transform. In either case, the superiority was observed across all performance indices. For completeness, we furnished optimal hyperparameters case-wise. Further, for each of the above detectors, an optimal variant minimized the validation loss at epoch 3 (with different and somewhat significant variances) as shown in Fig. 5.

The hierarchical classification test shows an overall strong end-to-end performance characterized by high values along the diagonal of the classification confusion matrix (table II), with an especially strong affinity for identifying high-quality images (eye present and well-lit, ground truth  $PL$ ) - images passing both tier 1 (eye presence) and tier 2 (satisfactory lighting). The confusion matrix shows that tier 1 (tasked with flagging all images with eye not present  $\bar{P}$ ) works with near-perfect performance. Majority of the misclassifications occurred because eye-present and badly-lit images ( $P\bar{L}$ ) were misclassified as eye-present and well-lit ( $PL$ ) which can be attributed to the need for improvement in tier 2. Grouping  $\bar{P}$  and  $P\bar{L}$  together as low-quality and taking  $PL$  as high-quality, we can view this as a binary classification result for quality assessment. For this binary classification, we obtain the performance metric values to be 91%, 0.9037, and 0.8244

TABLE II: Hierarchical classification confusion matrix for 'presence of eye' and 'lighting' features given 100 samples per ground truth label (fraction in parenthesis)

Ground Truths	Predicted $\bar{P}$	Predicted $P\bar{L}$	Predicted $PL$
$\bar{P}$	99 (0.99)	0 (0)	1 (0.01)
$P\bar{L}$	1 (0.01)	73 (0.73)	26 (0.26)
$PL$	0 (0)	0 (0)	100 (1)

for accuracy, P4 and Custom score respectively.

While related eyecare research usually attempt AI-based detection of specific eye diseases, such as Diabetic Retinopathy [7], development of a general quality assessment tool that apply to a broad spectrum of eye diseases has hitherto remained relatively less explored, possibly due to unavailability of disease-specific data for many diseases. In contrast and as a remedy, we approached the problem not from a disease-centric perspective but from an ocular structural perspective. The architecture for the above experiments was primarily adopted from works in eye-tracking [8], due to its focus on the eye structure within images, and majorly influenced by other AI-based biomedical solutions. In particular, this preliminary study was an effort toward assisting every teleconsultation with an AI-based tool that assesses captured images, possibly repeatedly and keep the subject ready with suffuciently high-quality ones, so that time and effort of the clinician is optimally utilized. The objective would be fully realized as we develop a comprehensive solution in future.

## REFERENCES

- [1] S. Iqbal, D. Ak, and G. Ds, "Blindness: Indian scenario: Is it really preventable," *Int J Med Res Rev*, vol. 1, no. 5, pp. 255–60, 2013.
- [2] A. Purohit, J. Smith, and A. Hibble, "Does telemedicine reduce the carbon footprint of healthcare? a systematic review," *Future Healthcare Journal*, vol. 8, no. 1, p. e85, 2021.
- [3] V. P. Joshi, A. Jain, R. Thyagrajan, and P. K. Vaddavalli, "Anterior segment imaging using a simple universal smartphone attachment for patients," *Seminars in ophthalmology*, 2022.
- [4] A. Krizhevsky, I. Sutskever, and G. E. Hinton, "Imagenet classification with deep convolutional neural networks," *Commun. ACM*, vol. 60, p. 84–90, may 2017.
- [5] L. Wang and Y. Sun, "Image classification using convolutional neural network with wavelet domain inputs," *IET Image Processing*, vol. 16, no. 8, pp. 2037–2048, 2022.
- [6] M. Sitarz, "Extending f1 metric, probabilistic approach," 10 2022.
- [7] E. Vocaturo and E. Zumpano, "The contribution of ai in the detection of the diabetic retinopathy," in *2020 IEEE International Conference on Bioinformatics and Biomedicine (BIBM)*, pp. 1516–1519, 2020.
- [8] M. M. Rahman, M. S. Islam, M. K. Ara Jannat, M. H. Rahman, M. Arifuzzaman, R. Sassi, and M. Aktaruzzaman, "Eyenet: An improved eye states classification system using convolutional neural network," in *2020 22nd International Conference on Advanced Communication Technology (ICACT)*, pp. 84–90, IEEE, 2020.